

## Tunable Filter-Antennas for Cognitive Radio Applications

Ali H. Ramadan<sup>1, \*</sup>, Joseph Costantine<sup>1</sup>, Mohammed Al-Husseini<sup>1</sup>, Karim Y. Kabalan<sup>1</sup>,  
Youssef Tawk<sup>2</sup>, and Christos G. Christodoulou<sup>3</sup>

**Abstract**—In this paper, frequency-tunable microstrip antennas, for cognitive radio applications, are proposed. The approach is based on electrically tuning the antenna’s operating frequency by integrating reconfigurable band pass filters into wideband antenna structures. The design of an open loop resonator (OLR)-based bandstop filter, and its transformation to a bandpass filter, are investigated first. Then, the incorporation of the bandpass filter, with a wideband antenna, is detailed. The same methodology is employed to design cognitive radio pattern and polarization diversity tunable filter-antennas. A good agreement between the simulated and measured results for the different fabricated prototypes is attained.

### 1. INTRODUCTION

A cognitive radio is capable of observing whether a specific frequency band is being allocated to a specific user or terminal. If the frequency band is found idle, then a cognitive radio can use that frequency band. This improves the spectrum usage efficiency, and allows the frequency bands to be always allocated to different users. If the authorized terminal (primary user) restarted transmission, the secondary terminal jumps off into a different band, or alters its transmission power level, modulation scheme, or its antenna’s radiation characteristics, while staying in the same frequency band, to suppress interference [1].

In [2], a survey of spectrum sensing methodologies for cognitive radio is presented. Besides studying the various aspects of spectrum sensing problem, and their associated challenges, a multidimensional spectrum sensing concept is introduced. Herein, the spectrum sensing term is declared as a general term that involves obtaining the spectrum usage characteristics across multiple dimensions such as time, space, frequency, and code. Other dimensions, such as location and angle of arrival need to be explored. The radio space with the introduced dimensions can be defined as a theoretical hyperspace occupied by radio signals, which has dimensions of location, angle of arrival, frequency, time, and possibly others.

In [2–5], the most common spectrum sensing techniques in the cognitive radio literature are given. These include energy detection, waveform-, cyclostationarity-, radio identification, matched-filtering and sub-sampling based sensing techniques. Cooperative sensing, whether it is centralized or distributed, is also proposed in [2, 3], as a solution to problems that arise in spectrum sensing due to noise uncertainty, fading, and shadowing. The implementation of a reconfigurable sensing methodology [6], may adjust itself to minimize the probability of wrongful detection. Thus, a reconfigurable sensing methodology may constitute an optimal spectrum sensing solution. On the other hand, RF receivers are expected to process narrowband baseband signals of the wide frequency spectrum with reasonably low complexity and low power processors. In other words, the RF components such as antennas, amplifiers, mixers and oscillators are expected to operate over a wide range of frequencies [2, 7].

---

*Received 20 November 2013, Accepted 13 December 2013, Scheduled 16 December 2013*

\* Corresponding author: Ali Halim Ramadan (ramadan@ieee.org).

<sup>1</sup> ECE Department, American University of Beirut (AUB), P. O. Box 11-0236, Bliss Street, Beirut 11072020, Lebanon. <sup>2</sup> ECCE Department, Notre Dame University-Louaize (NDU), P. O. Box 72, Zouk Michael, Lebanon. <sup>3</sup> ECE Department, University of New Mexico (UNM), Albuquerque, NM 87131, USA.

Unlike software-defined radios (SDRs), the cognitive radio (CR) counterparts are expected to sense the occupancy or target any channel in the entire spectrum, and tolerate interference at any frequency as well. These requirements generate constraints on antenna design, low-noise amplification, frequency synthesizers that provide a carrier frequency from tens of megahertz to about 10 GHz, mixing spurs, and spectrum sensing [8]. Upon employing tunable narrowband circuits rather than pursuing a truly wideband approach, the required flexibility of software-defined radio front-end may be met with better overall performance. Although having attractive features, a wideband front-end may not necessarily be the optimum solution for software-defined radio as it leads to a compromise in the transceiver performance, caused by limitations in the front-end components. Therefore, techniques of introducing flexible frequency discrimination, which include tunable bandpass, tunable bandstop filters and tunable narrowband antennas, help reduce spurious spectral content in the transmitter and limit out-of-band interference in the receiver [9].

Cognitive radio antennas, for overlay spectrum approaches, are usually dual-port antenna systems. Such antenna systems integrate a wideband antenna, used for sensing, with a frequency-reconfigurable antenna to communicate [10]. However, it is of a great importance to consider both mutual coupling reduction and polarization alignment between the two antennas in order to avoid any performance degradation. Another crucial issue to consider is the limitations of wideband antennas when it comes to spectrum sensing. Wideband antennas present an inherent gain-bandwidth product limitation, they also exhibit fluctuations resulting in a low signal to noise ratio. Wideband antennas require high-speed ADCs, which are power intensive and have higher quantization errors. The design for wideband operation leads to compromise in the transceiver performance, caused by limitations in the RF front-end components such as amplifiers, oscillators and mixers. As a solution to all the aforementioned issues in wideband antennas, narrowband frequency tunable antennas or tunable filter antennas appear as a more suitable solution for spectrum sensing. This is because tunable bandpass filtering provides flexible frequency discrimination, wideband suppression of unwanted interference, gain flatness over the operating frequency band, less disruption of the antenna's radiation characteristics, better processing of down-converted signals, and ease of implementation. Hence, a new cognitive radio antenna, for overlay spectrum operation, may be a single-port antenna system, which can be appropriately controlled to either sense or communicate.

Polarization spectrum holes sensing schemes allow adjusting the polarization of secondary users to limit interference to primary users. This results in higher throughput and spectral resources sharing in polarization domain [11–13]. Polarization diversity tunable filter-antennas provide simultaneous operation of primary and secondary users with less interference in an overlapped cognitive radio environment. On the other hand, pattern diversity tunable filter-antennas help combat multi-path fading and co-channel interference, while sensing the frequency spectrum. Thus, tunable filter-antennas with pattern or polarization diversity attributes add to the efficiency of spectrum sensing in cognitive radio networks.

In this paper, tunable filter-antennas for overlay cognitive radio applications are presented. A design approach, which is based on converting the wideband operation of an antenna into a tunable narrowband one via preselect filtering is discussed. A varactor-tuned bandpass filter is integrated into a wideband antenna to achieve frequency tuning without disturbing the radiation pattern. The SMV1405 varactor is utilized in this work. The same technique is employed to design pattern and polarization diversity tunable filter-antennas for cognitive radio applications.

Section 2 exploits OLRs to design a bandstop filter, and how it can be transformed to achieve a bandpass operation with tuning capability. It also discusses the integration of a tunable OLR-based bandpass filter into a wideband antenna. The proposed tunable filter-antenna for cognitive radio applications is presented in Section 3. Sections 4 and 5 discuss the design of cognitive radio pattern and polarization diversity tunable filter-antennas, respectively. The paper is concluded in Section 6.

## 2. OLR-BASED FILTER DESIGN

### 2.1. Negative Permeability Microstrip Transmission Lines

Rectangular or square shaped half wavelength open loop resonators are considered a type of split ring resonators. A microstrip transmission line loaded with OLRs behaves as a medium with a negative

permeability [14]. Fig. 1(a) shows a half-wavelength open loop resonator based on a 12 mm × 7.8 mm single-sided 1.6 mm-thick Taconic TLY substrate. The electrical length of the resonator is approximately 180° at 3.25 GHz. It is important to note that a bandstop operation appears in the vicinity of the OLR’s resonant frequency. This bandstop behavior is a consequence of the negative magnetic permeability properties of the structure. The negative magnetic permeability causes a strong mismatch at the resonant frequency of the OLR, thus resulting in a total reflection of the injected power. In order to extract the *S*-parameters of the resonating structure, the boundary conditions, as illustrated in Fig. 1(b), are considered. The computed *S*-parameters, using Ansoft HFSS, of the below OLR are depicted in Fig. 2. A method to retrieve the refractive index  $\eta$  and the wave impedance  $z$ , which are related to the magnetic permeability  $\mu$  by the relation  $\mu = \eta z$ , from the *S*-parameters of a *d*-thick slab is reported in [15]. Equations (1) and (2) can be used to find  $\mu$  in terms of the scattering parameters as follows.

$$\eta = \frac{1}{kd} \cos^{-1} \left[ \frac{1}{S_{21}} (1 - S_{11}^2 + S_{21}^2) \right] \tag{1}$$

$$z = \sqrt{\frac{(1 + S_{11})^2 - S_{21}^2}{(1 - S_{11})^2 - S_{21}^2}} \tag{2}$$

The retrieved normalized magnetic permeability ( $\mu_n$ ) of the unit cell, shown in Fig. 1, is depicted in Fig. 3. It is obvious that a negative real value of  $\mu$  is attained in the vicinity of the OLR’s resonant frequency. As a result, a microstrip transmission line loaded with the same OLR, as demonstrated in Fig. 4(a), behaves as a bandstop filter at 3.25 GHz. This is due to the negative magnetic permeability properties of the whole structure at the same frequency.

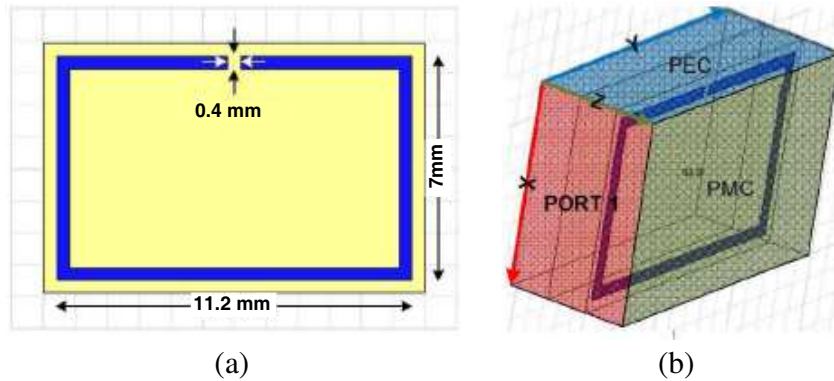


**Figure 1.** (a) Geometry and (b) boundary conditions of the half-wavelength open loop resonator.

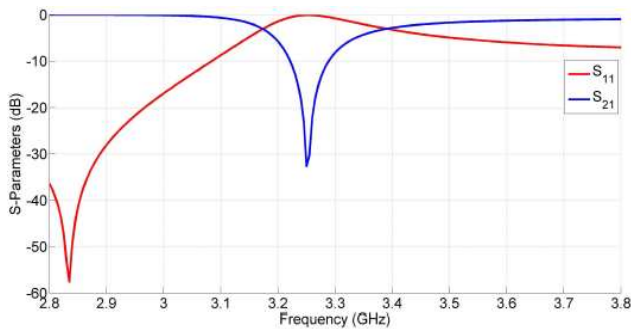


**Figure 2.** Computed *S*-parameters of the half-wavelength open loop resonator.

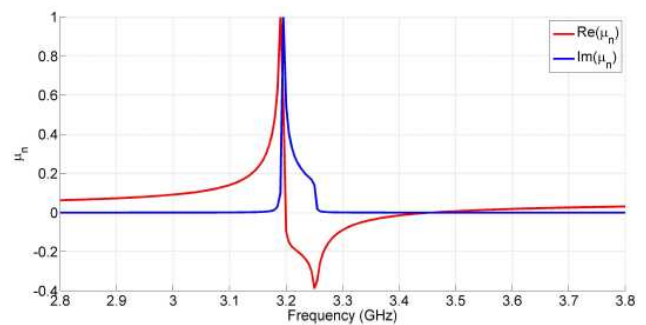


**Figure 3.** Normalized magnetic permeability ( $\mu_n$ ) of the unit cell in Fig. 1.

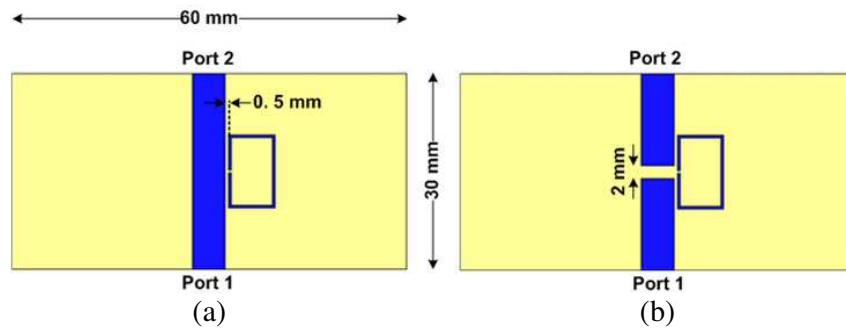


**Figure 4.** An OLR-based (a) bandstop filter and (b) bandpass filter.

## 2.2. An OLR-Based Bandpass Filter

A bandpass behavior is attained by etching a capacitive 2 mm-gap in the microstrip transmission line, as depicted in Fig. 4(b). According to [14], this combination is considered as a right-handed SRR/gap section, and provides forward signal propagation in the frequency band where both the permeability and the permittivity are positive. The series capacitance loaded in the line precludes transmission outside of the OLR's resonant frequency band. A prototype of each filter is shown in Fig. 5. A comparison between the simulated and measured  $S$ -parameters is depicted in Figs. 6 and 7, where a good agreement is attained.



**Figure 5.** A photo of the fabricated bandstop and bandpass filter prototypes.

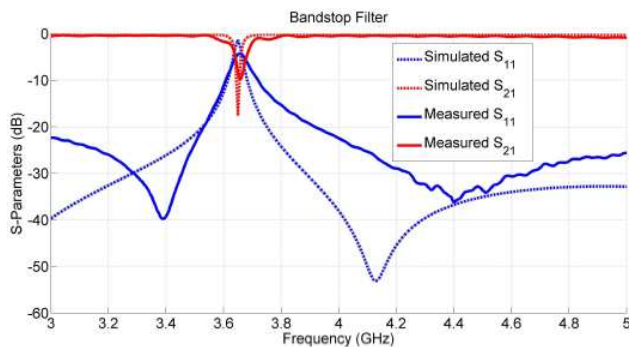


**Figure 6.** Simulated and measured  $S$ -parameters of the OLR-based bandstop filter.

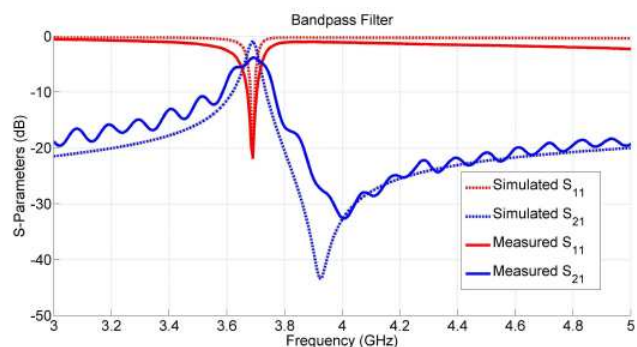


**Figure 7.** Simulated and measured  $S$ -parameters of the OLR-based bandpass filter.

## 2.3. Integration of an OLR-Based Bandpass Filter into a Wideband Antenna

A 3.41 GHz-operable OLR-based bandpass filter is firstly designed on a 1.6 mm-thick Taconic TLY substrate. The dimensions of the proposed filter are given in Fig. 8(a). A  $60 \times 60 \times 1.6 \text{ mm}^3$  Taconic

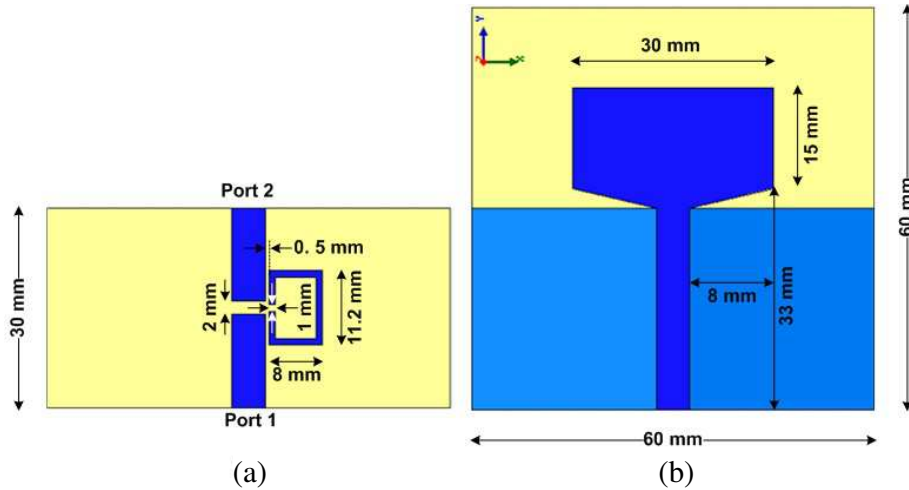


Figure 8. Geometry of the (a) the OLR-based bandpass filter and (b) wideband antenna.

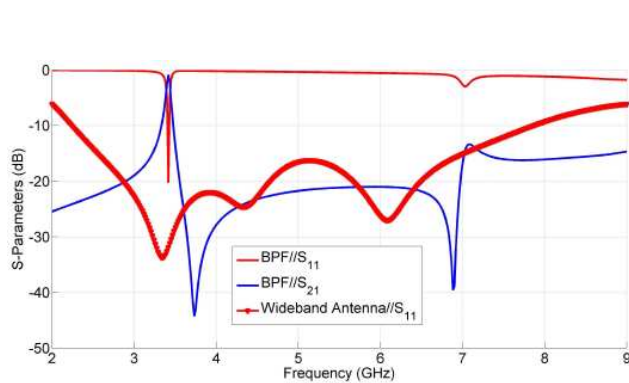


Figure 9. Computed *S*-parameters of the OLR-based bandpass filter and the wideband antenna.

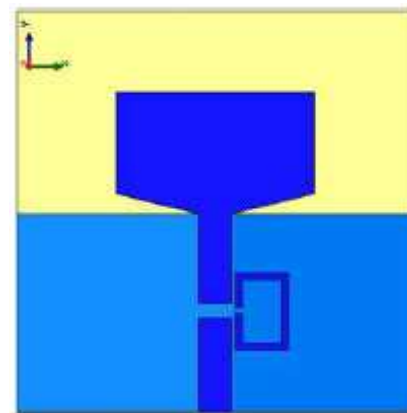


Figure 10. Integration of the OLR based bandpass filter into the wideband antenna.

TLY based wideband antenna is then designed as shown in Fig. 8(b). The antenna has a 30 mm-long partial ground plane flushed with a feed line. A tapered matching section is incorporated between the rectangular patch of the antenna and its feed line in order to achieve better impedance matching.

The computed *S*-parameters of the bandpass filter and the wideband antenna, in the 2–9 GHz frequency range, are shown in Fig. 9. The reflection coefficient of the antenna is  $\leq -10$  dB in the 2.24–7.86 GHz frequency range. Finally, both the OLR-based bandpass filter and the wideband antenna are assembled in a single structure, as illustrated in Fig. 10. The proposed filter-antenna is found to resonate, as shown in Fig. 11, at the same operating frequency of the contained bandpass filter.

### 3. A NARROWBAND FREQUENCY-TUNABLE ANTENNA FOR COGNITIVE RADIO APPLICATIONS

In order to achieve narrowband frequency tuning for the proposed filter-antenna, an SMV1405 varactor is incorporated onto the OLR of the bandpass filter. Increasing the capacitance of the varactor results in longer electrical lengths for OLRs. Correspondingly, the resonant frequency decreases in value. In other words, the adjustment of the reverse voltage across the bridging varactor will result in tuning the resonant frequency of the filter-antenna. The configuration of the proposed tunable filter-antenna, along with its biasing network, is given in Fig. 12.

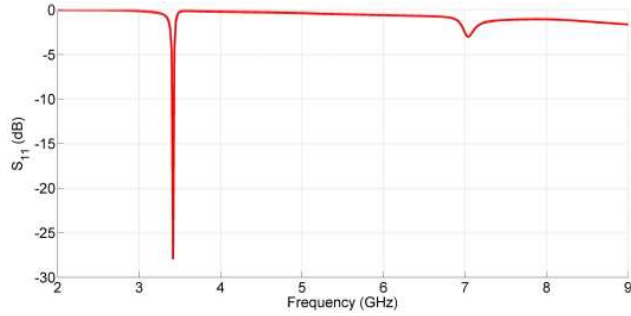


**Figure 11.** Simulated reflection coefficient of the assembled structure.

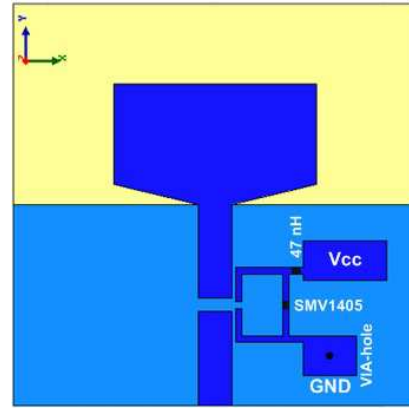


**Figure 12.** Configuration of the proposed tunable filter-antenna.

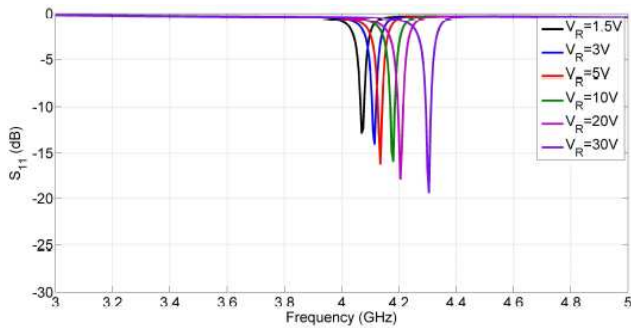


**Figure 13.** Simulated reflection coefficient of the proposed tunable filter-antenna.

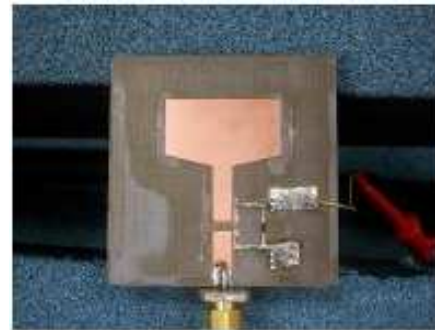


**Figure 14.** A fabricated prototype of the proposed tunable filter-antenna.

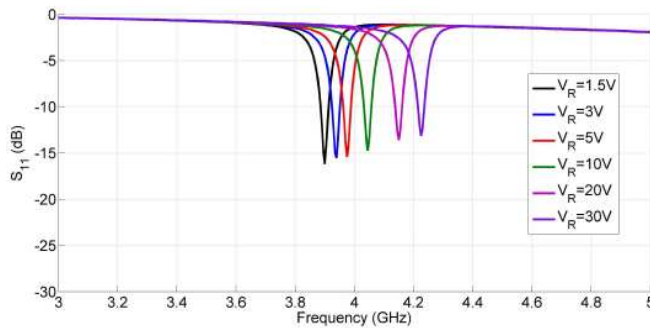


**Figure 15.** Measured reflection coefficient of the proposed tunable filter-antenna.

A 47 nH RF choke is incorporated to prevent any RF leakage to the DC supply. The other terminal of the tunable OLR is grounded through a via-hole. Accordingly, the Vcc and GND pads are used to adjust the reverse voltage across the mounted varactor. The computed reflection coefficient for different reverse voltages is shown in Fig. 13. It is worth mentioning that as the reverse voltage increases, the tunable filter-antenna resonates at higher frequencies. This is because the value of the loading capacitance is inversely proportional to the applied reverse voltage, and this yields a resonance at higher frequencies. A prototype of the designed tunable filter-antenna, as illustrated in Fig. 14, is fabricated and measured. A good analogy between simulated and measured plots is shown in Fig. 15. The normalized radiation patterns, of the wideband antenna and the proposed tunable filter-antenna, at

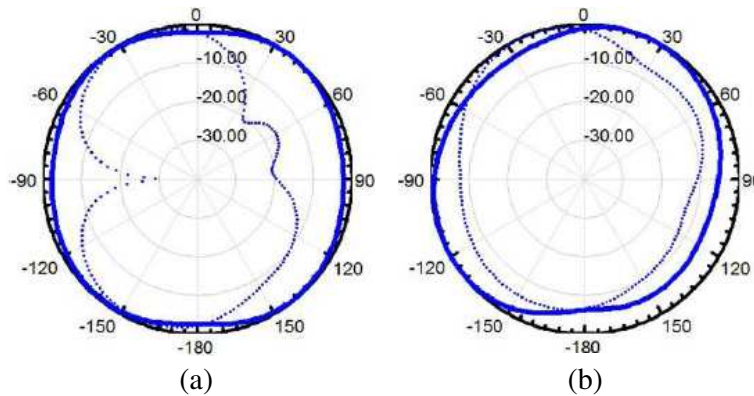


**Figure 16.** Normalized radiation pattern of (a) the wideband antenna and (b) the proposed tunable filter-antenna at 4.18 GHz ( $X$ - $Z$ / $Y$ - $Z$  plane: solid/dotted line).

4.18 GHz are depicted in Fig. 16. The radiation pattern of the tunable filter-antenna, in the  $X$ - $Z$  plane, is still omni-directional, and minimally distracted. Moreover, the gain of the tunable filter-antenna, at 4.18 GHz, is 4 dB, which is 1.86 dB higher than that of the wideband antenna at the same frequency.

#### 4. A FREQUENCY-TUNABLE PATTERN DIVERSITY ANTENNA FOR COGNITIVE RADIO APPLICATIONS

In a communications system implementing diversity, the same data is sent over independent fading paths. The signals received over the independent paths are then combined in such a way that the fading of the resultant signal is reduced. A wireless communication system equipped with diversity antennas leads to improved capacity and quality of the wireless channel [16]. In this section, a pattern diversity antenna, with a frequency tuning feature is presented. This will help combat multi-path fading and co-channel interference, while sensing the frequency spectrum.

The proposed 1.6 mm-thick Taconic TLY based pattern diversity tunable filter-antenna comprises two microstrip-line fed monopoles that are based on the same circular patch. Two symmetrically curved slots are etched in the ground plane. First, a circular slot with a radius of 8 mm is introduced below each patch, and then a  $10 \times 18 \text{ mm}^2$  rectangular slot is made at each of two corners. The etched curved slots direct the beams of the two monopoles in opposite azimuthal directions, leading to pattern diversity. A  $2 \times 20 \text{ mm}^2$  rectangular slot placed halfway between the monopoles is used to increase the isolation and adjust the antenna's operating frequency range. Two varactor-tuned half-wavelength OLR-based bandpass filters are then integrated into the pattern diversity antenna to achieve frequency tunability. The detailed structure of the proposed pattern diversity tunable filter-antenna is illustrated in Fig. 17.

The computed  $S$ -parameters for each reverse voltage of the bridging varactor are shown in Fig. 18. The simulation results reveal a narrowband frequency tunability, and an isolation better than 18 dB. It is worth mentioning that the incorporated ground configuration not only contributes to the mutual coupling reduction between the two monopoles, but also to their impedance bandwidth adjustment and radiation patterns orthogonality. Consequently, a tradeoff among the aforementioned issues is attempted to preserve the pattern diversity performance of the proposed tunable filter-antenna. A fabricated prototype of the proposed design is depicted in Fig. 19. The measured results are shown in Fig. 20. A slight and tolerable shift between the simulated and measured data is found due to the actual varactor component (SMV1405)'s modeling, and fabrication effects.

Figure 21 shows the normalized radiation patterns of the presented tunable filter-antenna at 3.72 GHz. It is seen that the patterns in the  $H$ -plane are symmetric and tend to cover complementary space region. With these patterns, the proposed design can provide pattern diversity over the operating frequencies. At 3.72 GHz, each monopole provides a peak gain of approximately 5 dB.

The diversity performance of an antenna system, as reported in [17–19], can be assessed by calculating the envelope correlation coefficient ( $\rho_e$ ) and the mean effective gain (MEG). The correlation

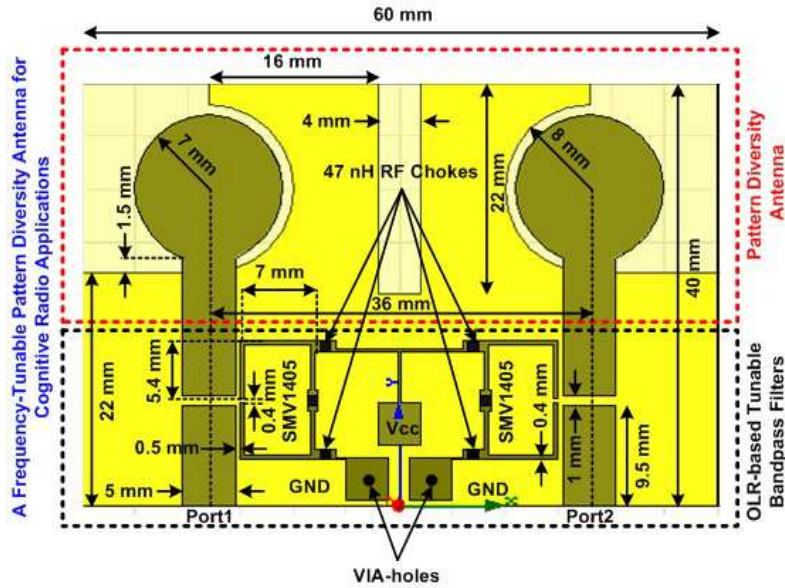


Figure 17. Configuration of the proposed pattern diversity tunable filter-antenna.

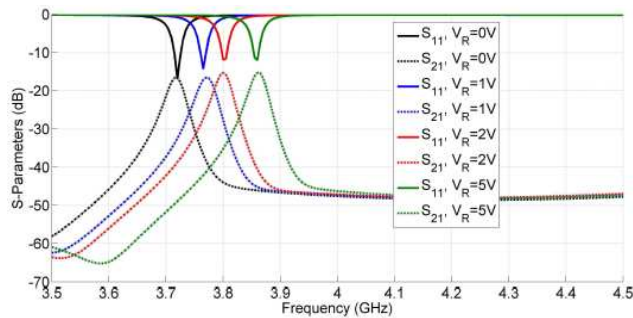


Figure 18. Simulated  $S$ -parameters of the proposed pattern diversity tunable filter-antenna.

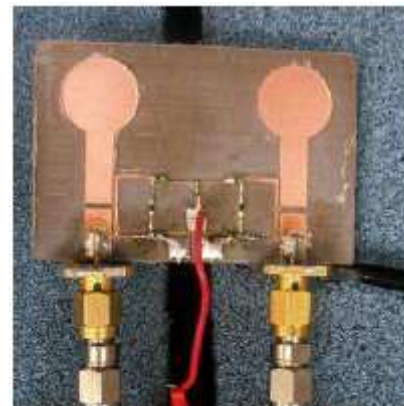


Figure 19. A fabricated prototype of the proposed pattern diversity tunable filter-antenna.

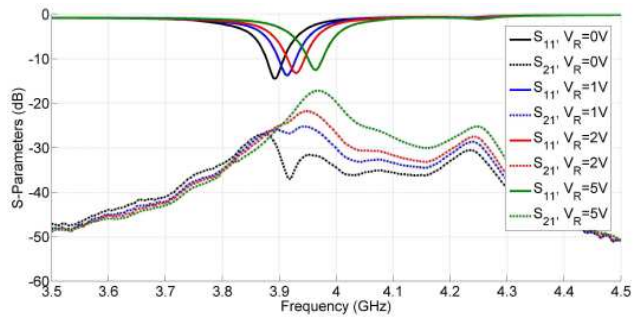


Figure 20. Measured  $S$ -parameters of the proposed pattern diversity tunable filter-antenna.

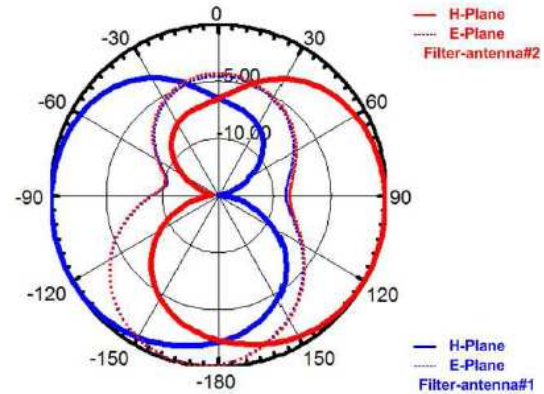


Figure 21. Normalized radiation pattern of the proposed pattern diversity tunable filter-antenna at 3.72 GHz.

coefficient shows the influence of the different propagation paths on the RF signals reaching the antenna elements. In a diversity system, a good gain can be obtained when  $\rho_e < 0.5$ .  $\rho_e$  relates to the mutual coupling between the antennas' ports as follows.

$$\rho_e = \frac{|S_{11}^* S_{12} + S_{21}^* S_{22}|^2}{(1 - |S_{11}|^2 - |S_{12}|^2)(1 - |S_{22}|^2 - |S_{21}|^2)} \quad (3)$$

The mean effective gain is a parameter that includes antenna radiation power pattern, antenna efficiency and the propagation effects. Equal power branches mean better condition for achieving high diversity gain. To guarantee that the signal strengths of the two monopoles are approximately equal, the ratio MEG1/MEG2 should be close to unity. For the proposed tunable filter-antenna, the conditions  $\rho_e < 0.5$  and MEG1/MEG2  $\simeq 1$  are both met, per operating frequency, as given in Table 1. As a result, a high diversity gain for the presented tunable filter-antenna is achieved.

$$MEG = \frac{1}{2\pi} \cdot \int_0^{2\pi} \left[ \frac{\Gamma \cdot G_\theta \left(\frac{\pi}{2}, \varphi\right) + G_\varphi \left(\frac{\pi}{2}, \varphi\right)}{1 + \Gamma} \right] d\varphi \quad (4)$$

**Table 1.** Diversity parameters of the proposed tunable filter-antenna.

Frequency (GHz)	3.72	3.765	3.8	3.86
$\rho_e \ll 0.5$	$6214 \times 10^{-7}$	$101 \times 10^{-4}$	$7489 \times 10^{-7}$	$3144 \times 10^{-6}$
MEG1/MEG2 $\simeq 1$	0.9952	1.0066	0.9915	0.9899

## 5. A FREQUENCY-TUNABLE POLARIZATION DIVERSITY ANTENNA FOR COGNITIVE RADIO APPLICATIONS

Polarization reconfigurable antennas help increase the performance of communications systems through polarization diversity and frequency reuse [20]. Few polarization reconfigurable antennas have recently been reported in the literature. This is due to the fact that good impedance matching is difficult to obtain over the desired frequency for various polarizations. To exploit polarization diversity as a reliable dimension in cognitive radio networks, frequency tuning is a must. The polarization match/mismatch among the tunable filter-antenna terminals of primary and secondary users not only increases the spectrum usage efficiency, but also suppresses interference at the same frequency. In this section, a narrowband frequency-tunable polarization diversity antenna is presented. The design approach is based on integrating tunable OLR-based bandpass filters with a polarization diversity antenna. Thus, polarization orthogonality per frequency band of operation is attained for the presented tunable filter-antenna.

The proposed polarization diversity tunable filter-antenna comprises two asymmetrically microstrip-line fed monopoles that are symmetrical in structure as shown in Fig. 22. It is based on a  $80 \times 192 \times 1.6 \text{ mm}^3$  Taconic TLY substrate. The patch of each monopole is designed as follows. A  $25 \text{ mm} \times 20 \text{ mm}$ -sized rectangle is intersected with a circle to obtain the round comers. The circle is co-centered with the rectangle, and has a radius of 13 mm. For each monopole, a  $1 \text{ mm} \times 20 \text{ mm}$  rectangular slit is etched in the  $30 \text{ mm} \times 80 \text{ mm}$  ground plane. A  $2.5 \text{ mm} \times 14.5 \text{ mm}$  loading stub is embedded next to each slit. This ground plane configuration contributes radiation pattern orthogonality in the opposite azimuth directions of the two monopoles. A  $29 \times 32 \text{ mm}^2$  rectangular slot is incorporated to minimize coupling between the monopoles. Two varactor-tuned OLR-based bandpass filters are then integrated into the polarization diversity antenna to achieve frequency tunability.

Figure 23 depicts the simulated  $S$ -parameters of the designed tunable filter-antenna for several varactor reverse voltage (loading capacitance) values. A prototype of the designed tunable filter-antenna is fabricated as shown in Fig. 24. A good agreement between simulated and measured results is shown in Fig. 25. Accordingly, a narrowband frequency tunability, and an isolation better than 20 dB are witnessed. Fig. 26 illustrates the normalized radiation patterns of the presented tunable filter-antenna at 3.7 GHz. It is seen that the patterns are symmetric and orthogonal in the  $H$ -plane. At 3.7 GHz, each monopole provides a peak gain around 4 dB.

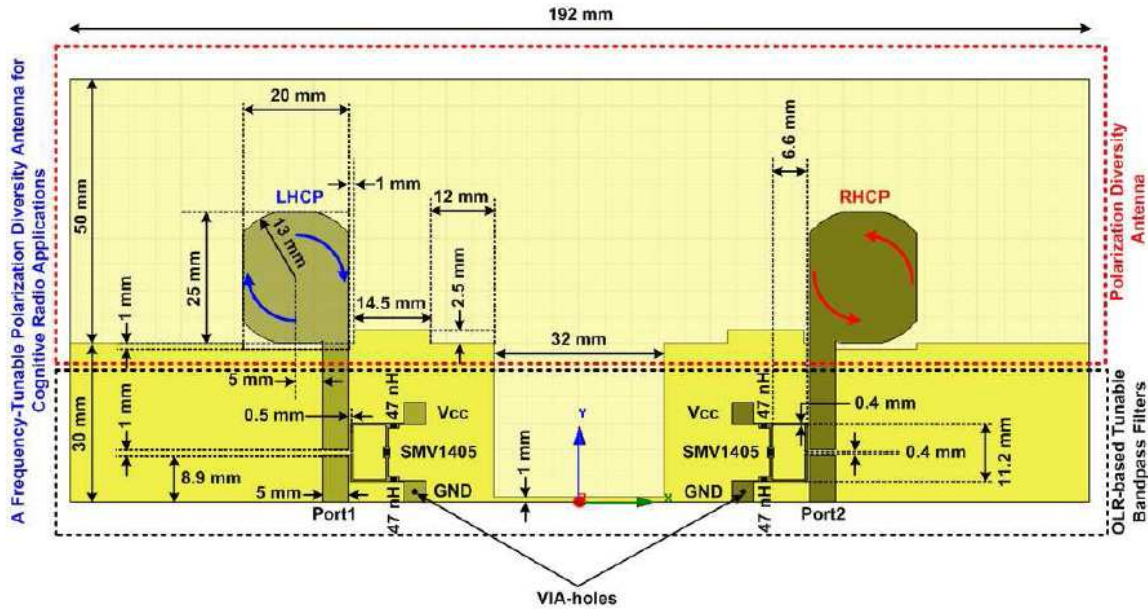


Figure 22. Configuration of the proposed polarization diversity tunable filter-antenna.

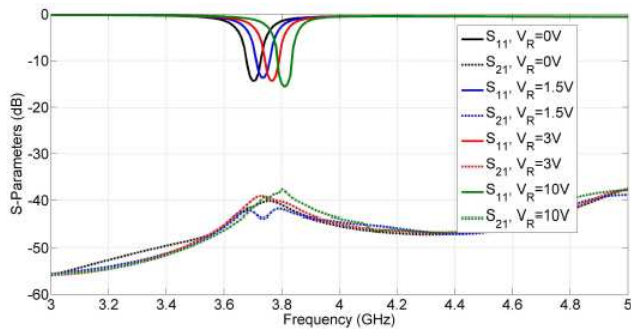


Figure 23. Simulated  $S$ -parameters of the proposed polarization diversity tunable filter-antenna.

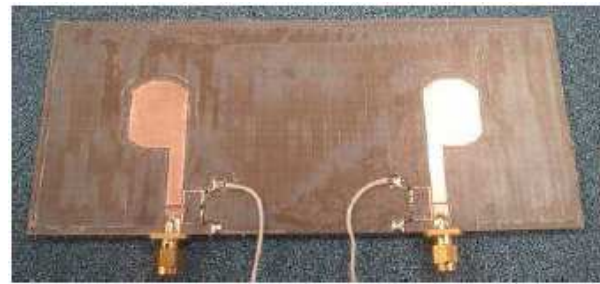


Figure 24. A fabricated prototype of the proposed polarization diversity tunable filter-antenna.

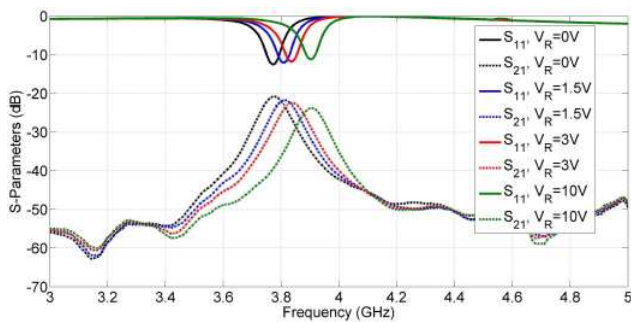


Figure 25. Measured  $S$ -parameters of the proposed polarization diversity tunable filter-antenna.

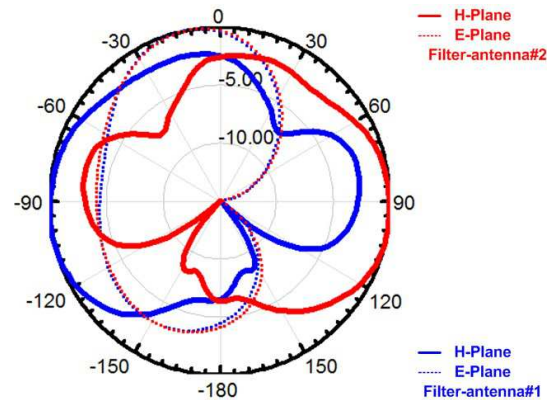


Figure 26. Normalized radiation pattern of the proposed polarization diversity tunable filter-antenna at 3.7 GHz.

To achieve equal amplitudes and a leading/lagging  $90^\circ$  phase difference between the vertical and horizontal electric fields distributed on the patch surface, a slit is etched in the ground plane [21]. This slit alters the surface current compactness and phasing on the patch to generate orthogonal electric fields ( $E_{Vertical}$  and  $E_{Horizontal}$ ) that meet circular polarization conditions. For instance, the etched slit beneath the patch of the tunable filter-antenna #1 results in almost equal amplitudes for  $E_{Horizontal}$  and  $E_{Vertical}$  with the latter led by a  $90^\circ$  shift to acquire LHCP radiation. Being symmetrical in structure, tunable filter-antenna #2 reveals RHCP radiation using the same methodology. Furthermore, the incorporated round corners in the patches help smoothing the flow of the circular surface current distribution for either polarization. The loading perturbation stubs, next to each slit, are embedded to achieve good impedance matching, over the desired frequency range, for both polarizations. At each operating frequency, the

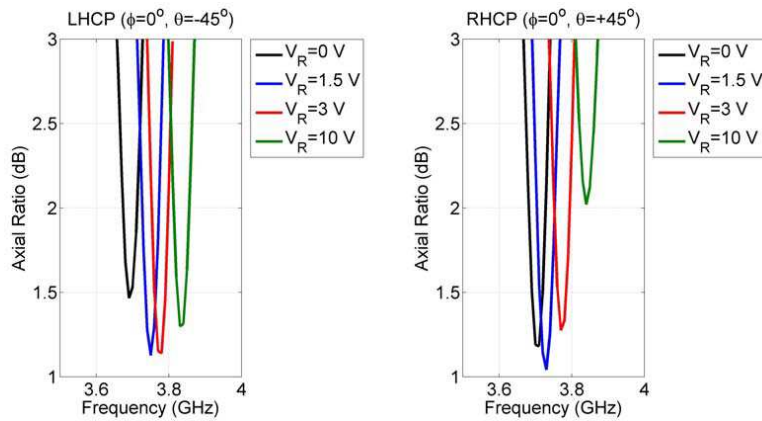


Figure 27. Axial ratio of the proposed polarization diversity tunable filter-antenna.

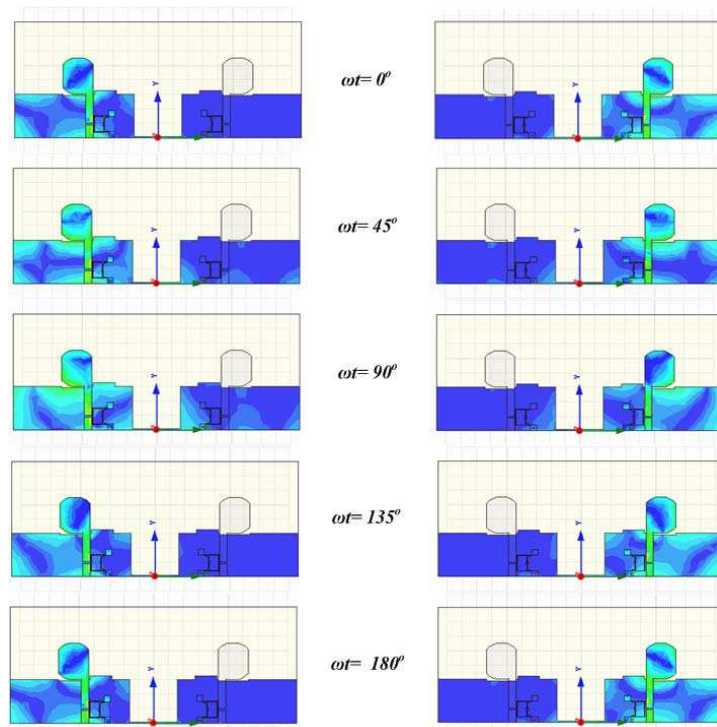


Figure 28. Electric field distribution of the proposed polarization diversity tunable filter-antenna for several reference phases at 3.7 GHz.

axial ratio (AR) of the tunable filter-antennas #1 and #2 in the respective ( $\varphi = 0^\circ$ ,  $\theta = -45^\circ$ ) and ( $\varphi = 0^\circ$ ,  $\theta = +45^\circ$ ) directions is less than 3 dB as given in Fig. 27.

Figure 28 illustrates the electric field distribution of the proposed design for several reference phases ( $\omega t = 0^\circ\text{--}180^\circ$ ) at 3.7 GHz. Therefore, both LHCP and RHCP radiations are revealed per the same operable frequency. As a result, a polarization diversity for the presented tunable filter-antenna is achieved.

## 6. CONCLUSION

In this paper, tunable filter-antennas for overlay cognitive radio applications are presented. The exploitation of OLRs to design a bandstop filter, and its transformation to a tunable bandpass filter is discussed. The integration of such a filter into a wideband antenna is reported. The proposed approach is based on integrating varactor-tuned half-wavelength OLR-based bandpass filter(s) into wideband antennas to electrically tune their resonant frequencies.

A narrowband frequency-tunable microstrip antenna is designed and tested at first. The same methodology is employed to design pattern and polarization diversity tunable filter-antennas for overlay cognitive radio applications.

For the pattern diversity antenna, the computed envelope correlation coefficient ( $\rho_e \ll 0.5$ ) and mean effective gain ratio (MEG1/MEG2  $\simeq 1$ ) at the operating frequencies revealed a high diversity gain. Two varactor tuned half-wavelength OLRs are also incorporated into the proposed polarization diversity tunable filter-antenna. The normalized radiation patterns of the presented tunable filter-antenna are symmetric and orthogonal in the  $H$ -plane. The axial ratio (AR) values of the tunable filter-antenna in the ( $\varphi = 0^\circ$ ,  $\theta = -45^\circ$ ) and ( $\varphi = 0^\circ$ ,  $\theta = +45^\circ$ ) directions are shown to be less than 3 dB.

## ACKNOWLEDGMENT

The authors gratefully acknowledge the support of Mr. Issam Darwish and Mr. Mohammad Darwish for the Electromagnetic and Radio Frequency Group (EMRF) at the American University of Beirut (AUB).

## REFERENCES

1. Kitsunezuka, M., K. Kunihiro, and M. Fukaishi, "Efficient use of the spectrum," *IEEE Microwave Magazine*, Vol. 13, No. 1, 55–63, 2012.
2. Yucek, T. and H. Arslan, "A survey of spectrum sensing algorithms for cognitive radio applications," *IEEE Communications Surveys Tutorials*, Vol. 11, No. 1, 116–130, 2009.
3. Axell, E., G. Leus, and E. G. Larsson, "Overview of spectrum sensing for cognitive radio," *2010 2nd International Workshop on Cognitive Information Processing (CIP)*, 322–327, Elba, Italy, June 14–16, 2010.
4. Weifang, W., "Spectrum sensing for cognitive radio," *Third International Symposium on Intelligent Information Technology Application Workshops (IITAW)*, 410–412, Nanchang, China, November 21–22, 2009.
5. Kwan, A., S. A. Bassam, and F. M. Ghannouchi, "Sub-sampling technique for spectrum sensing in cognitive radio systems," *IEEE Radio and Wireless Symposium (RWS)*, 347–350, Santa Clara, CA, USA, January 15–18, 2010.
6. Weingart, T., G. V. Yee, D. C. Sicker, and D. Grunwald, "Implementation of a reconfiguration algorithm for cognitive radio," *2nd International Conference on Cognitive Radio Oriented Wireless Networks and Communications (CROWNCOM)*, 171–180, Orlando, FL, USA, August 1–3, 2007.
7. Cabric, D. and R. W. Brodersen, "Physical layer design issues unique to cognitive radio systems," *IEEE 16th International Symposium on Personal, Indoor and Mobile Radio Communications (PIMRC)*, Vol. 2, 759–763, Berlin, Germany, September 11–14, 2005.
8. Razavi, B., "Challenges in the design of cognitive radios," *IEEE Custom Integrated Circuits Conference (CICC)*, 391–398, San Jose, CA, USA, September 13–16, 2009.

9. Carey-Smith, B. E., P. A. Warr, P. R. Rogers, M. A. Beach, and G. S. Hilton, "Flexible frequency discrimination subsystems for reconfigurable radio front-ends," *EURASIP Journal on Wireless Communications and Networking*, Vol. 2005, No. 3, 354–363, 2005.
10. Al-Husseini, M., A. El-Hajj, Y. Tawk, K. Y. Kabalan, and C. G. Christodoulou, "A simple dual-port antenna system for cognitive radio applications," *International Conference on High Performance Computing and Simulation (HPCS)*, 549–552, Caen, France, June 28–July 2, 2010.
11. Fangfang, L., C. Feng, C. Guo, W. Yue, and D. Wei, "Polarization Spectrum Sensing Scheme for Cognitive Radios," *5th International Conference on Wireless Communications, Networking and Mobile Computing (WiCom)*, 1–4, Beijing, China, September 24–26, 2009.
12. Wei, D., C. Guo, L. Fangfang, and Z. Zeng, "A SINR improving scheme based on optimal polarization receiving for the cognitive radios," *IEEE International Conference on Network Infrastructure and Digital Content (IC-NIDC)*, 100–104, Beijing, China, November 6–8, 2009.
13. Dricot, J., G. Ferrari, F. Quitin, A. Panahandeh, F. Horlin, and P. De Doncker, "Polarization orthogonality for the co-existence of wideband fading cognitive networks," *Proceedings of the Fifth International Conference on Cognitive Radio Oriented Wireless Networks Communications (CROWNCOM)*, 1–5, Cannes, France, June 9–11, 2010.
14. Marques, R., F. Martin, and M. Sorolla, *Metamaterials with Negative Parameters: Theory, Design and Microwave Applications*, John Wiley & Sons, Inc., Hoboken, New Jersey, 2008.
15. Smith, D. R., D. C. Vier, T. Koschny, and C. M. Soukoulis, "Electromagnetic parameter retrieval from inhomogeneous metamaterials," *Physical Review E*, Vol. 71, No. 3, 036617-1–036617-11, 2005.
16. Goldsmith, A., *Wireless Communications*, Cambridge University Press, New York, 2005.
17. Vaughan, R. G. and J. B. Andersen, "Antenna diversity in mobile communications," *IEEE Transactions on Vehicular Technology*, Vol. 36, No. 4, 149–172, 1987.
18. Yuan, D., Z. Du, K. Gong, and Z. Feng, "A novel dual-band printed diversity antenna for mobile terminals," *IEEE Transactions on Antennas and Propagation*, Vol. 55, No. 7, 2088–2096, 2007.
19. Al-Husseini, M., A. Ramadan, K. Y. Kabalan, A. El-Hajj, and C. G. Christodoulou, "A novel printed diversity antenna for WiMAX applications," *IEEE International Symposium on Antennas and Propagation (APS/URSI)*, 2212–2214, Spokane, WA, USA, July 3–8, 2011.
20. Qin, P. -Y., A. R. Weily, Y. J. Guo, and C.-H. Liang, "Polarization reconfigurable U-slot patch antenna," *IEEE Transactions on Antennas and Propagation*, Vol. 58, No. 10, 3383–3388, 2010.
21. Wu, J. -W., J.-Y. Ke, C. F. Jou, and C.-J. Wang, "Microstrip-fed broadband circularly polarised monopole antenna," *IET Microwaves, Antennas & Propagation*, Vol. 4, No. 4, 518–525, 2010.